Photophysical and Electrochemical Study of New Luminescent and Redox-Active Tetrazine Derivatives Grafted on Gold Nanoparticles

Livio Oliveira de Miranda, Baptiste Maillot, Margarita Bosmi, Laurent Galmiche, Jean-Frédéric Audibert, Philippe Decorse, Vitor Brasiliense, Léa Berthelier, Isabelle Bonnamour, Ulrich Darbost, et al.

Synthesis and Grafting of New Luminescent and Redox-Active Tetrazine Derivatives on Gold Nanoparticles

Livio Oliveira de Miranda, Baptiste Maillot, Margarita Bosmi, Laurent Galmiche, Jean-Frédéric Audibert, Vitor Brasiliense, Léa Berthelier[2], Isabelle Bonnamour[1], Ulrich Darbost[2], Fabien Miomandre*

Université Paris-Saclay, Ecole Normale Supérieure Paris-Saclay, CNRS, PPSM, 4 avenue des Sciences 91190 GIF-SUR-YVETTE (France)

Abstract

New tetrazine derivatives able to be grafted on gold surfaces have been synthesized with disulfide or thioctic anchoring units, and their electrochemical and photophysical properties investigated in solution. In parallel, gold nanoparticles have been electrodeposited on indium tin oxide surfaces and then functionalized by the tetrazine compounds. The modified surfaces have been characterized by XPS with a focus on the influence of the deposition potential and immersion time. Tetrazines remain fully electroactive and emissive once grafted. Electrochemical characterization shows that monolayers of tetrazine are formed with high values of the electron transfer rate. The photophysical study allows us to estimate the optimal deposition time and shows a gradual bleaching under continuous excitation which can be used to discriminate the contribution of the grafted fluorophores from the background and which is strongly dependent on the excitation power.

Introduction

Plasmonic substrates made of gold nanoparticles (Au NPs) on a conductive transparent substrate like indium tin oxide (ITO) are now well mastered to be used as electrodes for photoelectrochemical investigations or sensor applications. They can be designed using several techniques from the simplest ones (electrodeposition[1-6]) to the most sophisticated (lithography)[7-12]. The former ones have the advantage to be cheap and easy to be implemented, sometimes without any surfactant or additives, while the latters lead to well controlled and ordered assemblies with tunable sizes, shapes and inter-

[1] Institut de Chimie et Biochimie Moléculaires et Supramoléculaires, Université Lyon 1, 1 rue V. Grignard 69600 VILLEURBANNE (France)
[2] Institut Lumière Matière, Université Lyon 1, 10 rue Ada Byron, 69622 VILLEURBANNE (France)

particle distances. These substrates can be post-functionalized by molecular compounds using various methods among which self-assembly through sulfur containing anchoring groups have been probably the most popular. This way, various redox active moieties like ferrocene[13] or metal complexes[14] have been introduced on the surface with noticeable impact of the anchoring group[15] and chain length[16] on the final electrochemical properties.

Tetrazine derivatives have become a topic of interest due to their bioconjugaison ability using cycloaddition[17] but also because they are at the same time electroactive in a moderate potential range and emissive in the visible, thus conferring them electrofluorochromic properties[18]. Examples where tetrazine derivatives were used in combination with gold nanoparticles are not very numerous in the literature and limited to inverse demand Diels-Alder cycloaddition reactions in which the tetrazine ring is not preserved at the end.[19] One of the rare examples of Au NPs functionalized by organic ligands terminated by a tetrazine ring has been reported by Lennox et al.[20] involving a two-step procedure : functionalization of Au NPs by an hydroxyl terminated thiolate ligand followed by a nucleophilic substitution by dichlorotetrazine. One of the main difficulties encountered when trying to incorporate tetrazine rings at the surface of Au NPs is the incompatibility between the tetrazine as an electrophilic unit and the commonly used thiolate ligands having nucleophilic properties. To circumvent this, we propose a reaction pathway consisting in designing tetrazine derivatives containing either disulfide or thioctic (lipoic) units which are likely to be transformed into thiolates when put in presence of gold. This allows the direct functionalization of Au NPs with tetrazine terminated ligands, to generate conductive surfaces bearing both a redox active and a luminescent unit. Several tetrazine derivatives have been envisaged (scheme 1) for that purpose and their electrochemical and photophysical properties explored in a first step. Then, their ability to be grafted on the Au NPs surface has been checked and the resulting redox and photophysical properties of the functionalized monolayers investigated.

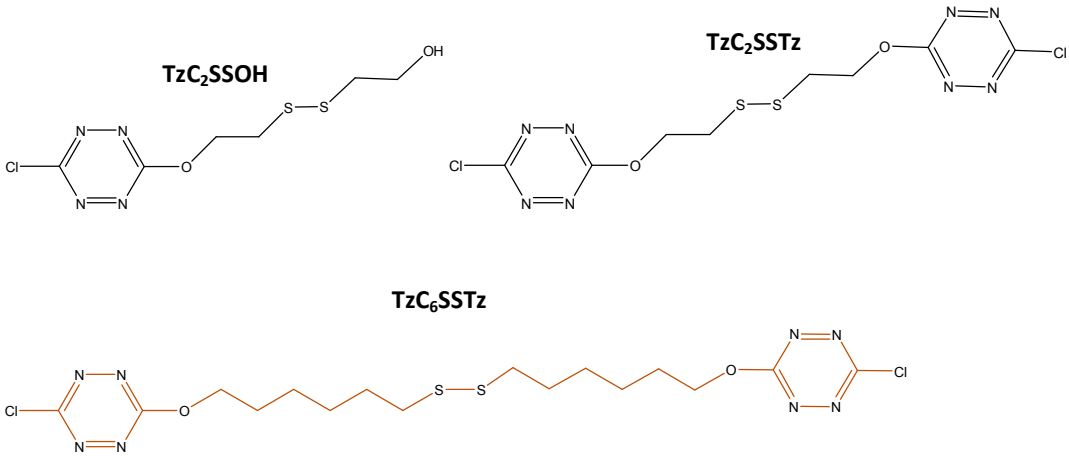

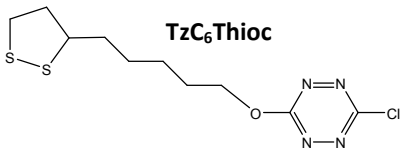

Scheme 1 : Formulae of the tetrazine derivatives bearing sulfur containing anchoring groups.

Results and discussion

1. Synthesis of the molecules

a) Disulfide derivatives

The disulfide tetrazine derivatives **TzC_6SSTz** and **TzC_2SSTz** were synthesized by reacting the corresponding dithiobis-alcohols and 3,6-dichloro-1,2,4,5-tetrazine in presence of 2,4,6-collidine as shown in Scheme 2. Firstly, 2,2'-dithiobis[ethanol] **$diSC_2OH$** and 6,6'-dithiobis[1-hexanol] **$diSC_6OH$** were obtained according to the literature protocol[21].

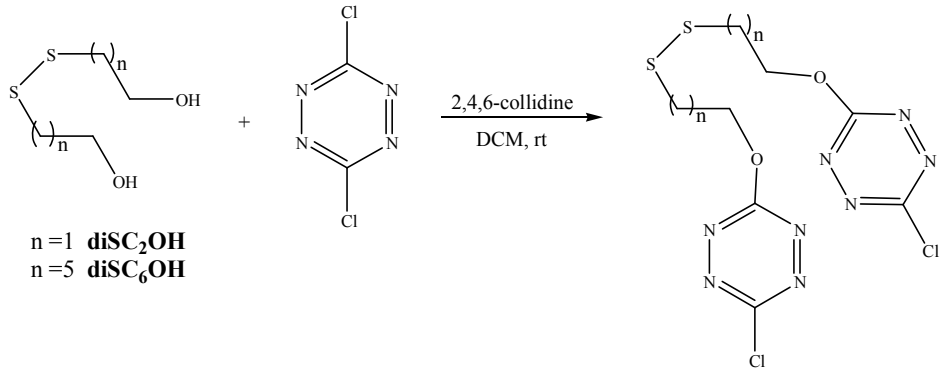

Scheme 2 : Synthesis of the disulfide tetrazine derivatives.

Then when the 3,6-dichloro-1,2,4,5-tetrazine was added to the disulfide compounds, we observed an orange color changing to dark red when collidine is added. Both **TzC_6SSTz** and **TzC_2SSTz** compounds were purified by silica gel column chromatographies. Using the same protocol and by varying the relative amounts of starting compounds, a single tetrazine unit can been grafted on the 2,2'-dithiobis[ethanol] $diSC_2OH$ leading to the monotetrazine derivative **TzC_2SSOH.**

Detailed protocols and NMR/MS features can be found in ESI.

b) Thioctic derivative

The compound **TzC$_6$Thioc** is obtained in two steps. The first one is the synthesis of 1,2 dithiolane-3-pentanol (lipolol) from the corresponding acid (thioctic acid).[22] In a second step, the lipolol, dichlorotetrazine and collidine are mixed in dichloromethane to obtain the target compound. Protocol details and NMR features of the product can be found in ESI.

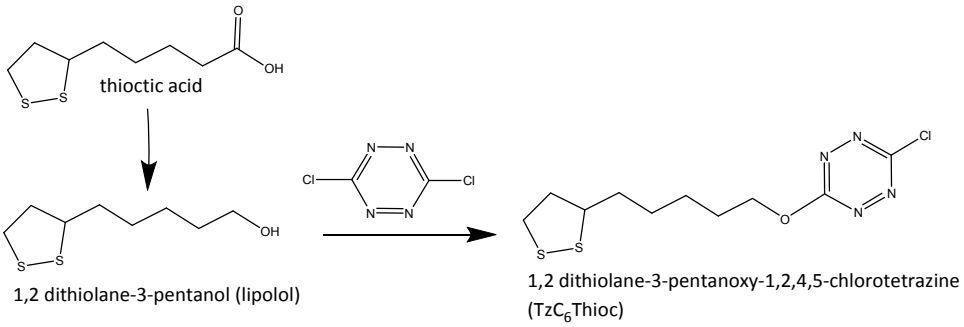

Scheme 3: Two-step route for the synthesis of TzC$_6$Thioc

2. Electrochemical and photophysical properties of the molecules in solution

Figure 1 shows the cyclovoltammogram (CV) obtained for two molecules of this series, namely **TzC$_6$SSTz** and **TzC$_6$Thioc** (CVs for the others can be found in Figure S1). One can recognize the typical features of the tetrazine electrochemistry with an almost perfectly reversible signal and a reduction located at ca. -0.7 V vs. Ag^+/Ag, which perfectly corresponds to the expected range for chloroalkoxytetrazines.[23] This first result shows that the electroactivity of the tetrazine unit is well preserved in the disulfide and thioctic compounds. To go further, it appears interesting to investigate if the observed electrochemical response actually corresponds to the number of tetrazine units present in the molecule. This can be done by varying the scan rate and measuring the diffusion coefficient from the analysis of the peak current vs. square root of scan rate (Randles equation).

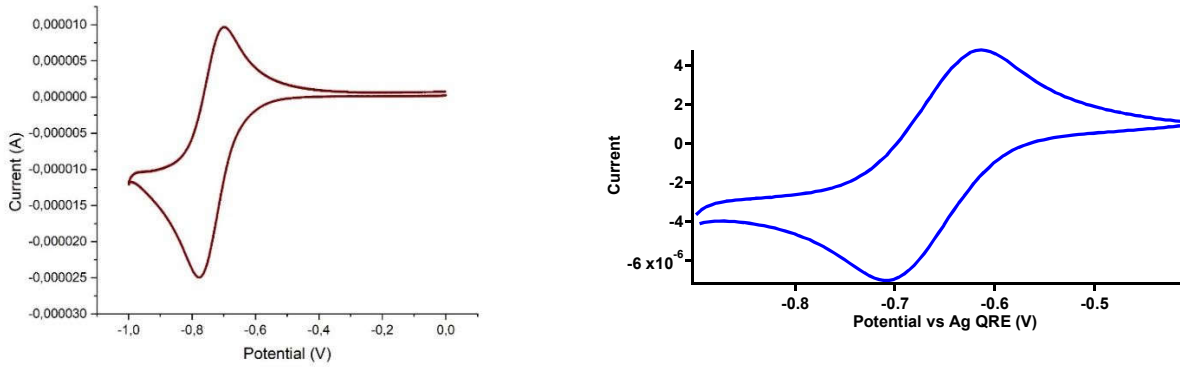

Figure 1: CVs of **TzC_6SSTz** (left) and **TzC_6Thioc** (right) 1 mM in acetonitrile on a gold disk electrode (diameter: 2 mm). Scan rate: 100 mV s^{-1}.

Table 1 shows the diffusion coefficient values extracted from the Randles analysis. Importantly, these calculations have been done assuming the number of electrons exchanged is equal to the number of tetrazine units present. Molecular sizes have been estimated from molecular dynamics and energy minimization for each compound in its non-solvated form (figure 2), in order to see if the diffusion coefficient values scale with the inverse of the size as predicted by the Stokes-Einstein model.

The results show that the diffusion coefficients D obtained vary linearly with the inverse of the size of the molecule d_{calc}, except for **TzC_6SSTz** for which the diffusion coefficient lies out of the straight line predicted by the Stokes-Einstein model (see figure S2 for the plot of D vs. $1/d_{calc}$). This exception is not really surprising since the shape of the molecule is much closer to a rod than to a sphere and thus the Stokes-Einstein model does not fit well in that case. Moreover, the slope of the linear fit in figure S2 is found to be very close to the theoretical value ($k_BT/(6\pi\eta) \approx 7.3\ 10^{-13}$ cm^3s^{-1} where k_B is the Boltzmann constant and η the solvent viscosity). This result confirms the validity of the initial assumption concerning the number of electrons exchanged. Therefore, we can estimate that all tetrazine units are actually redox active in the investigated derivatives of this series.

Table 1: Diffusion coefficients[a] in acetonitrile and estimated molecular diameters.

	TzC_2SSOH	**TzC_2SSTz**	**TzC_6SSTz**	**TzC_6Thioc**
D / 10^{-5} cm^2 s^{-1}	0.56	0.39	0.19	0.46
d_{calc} / Å	13.2	18.5	17.9	15.9

[a] assuming the number of electrons is equal to the number of tetrazine units.

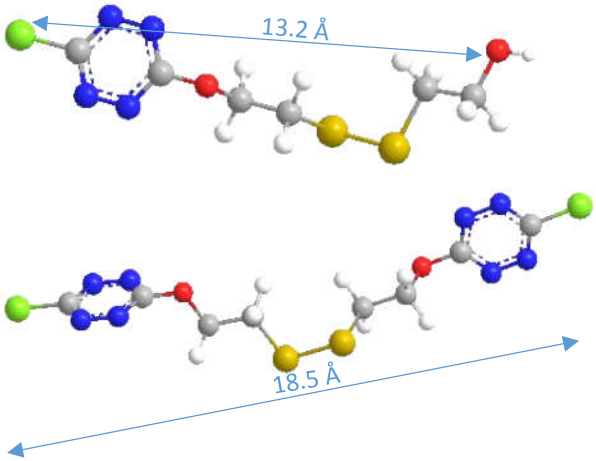

Figure 2: Representation of the molecules with their end to end distance after molecular dynamics and energy minimization.

The absorption and emission spectra of **TzC$_6$SSTz** and **TzC$_6$Thioc** are reported in figure 3 (see figure S3 for those of **TzC$_2$SSTz** and **TzC$_2$SSOH**), as well as the fluorescence decay recorded at the emission maximum in each case. As for electrochemistry, all the features recorded are those expected for a tetrazine derivative, namely two absorption bands (one in the UV and one less intense in the visible) and an emission band with a maximum located around 570 nm. The luminescence lifetime found for the disulfide derivative is in the expected range for a tetrazine compound, while the thioctic one is significantly lower (see table 2).

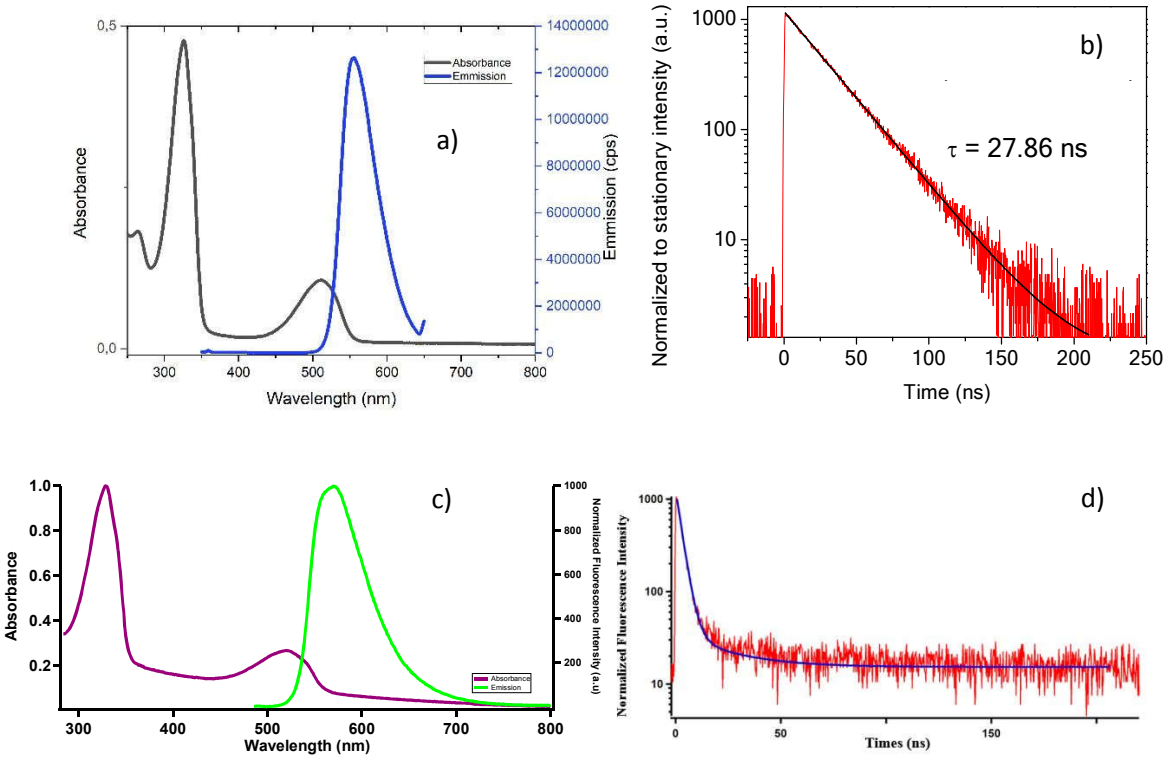

Figure 3: Absorption and photoluminescence spectra (λ_{exc} =325nm) of a) **TzC$_6$SSTz** and c) **TzC$_6$Thioc** (1 mM in acetonitrile). Fluorescence decay of b) **TzC$_6$SSTz** and d) **TzC$_6$Thioc** (1 mM in acetonitrile and fit by a monoexponential function).

Fluorescence quantum yields have been measured for all compounds in acetonitrile and the results are reported in table 2. The disulfide containing compounds show the lowest values, especially those with the shortest alkyl chains, while **TzC$_6$Thioc** displays a luminescence yield closer to the typical values recorded for chloroalkoxytetrazines (e.g. 0.23 for chloromethoxytetrazine).[23]

Based on these results, we selected **TzC$_6$SSTz** and **TzC$_6$Thioc** for further grafting on gold nanoparticles electrodeposited on ITO.

Table 2: Molar extinction coefficients at 520 nm (ε), fluorescence quantum yields (ϕ_{fluo}, measured at λ_{exc} = 520 nm) and lifetime (τ_{PL}) for all compounds in acetonitrile.

	TzC$_2$SSOH	**TzC$_2$SSTz**	**TzC$_6$SSTz**	**TzC$_6$Thioc**
ε / L mol^{-1} cm^{-1}	380	1250	530	940
ϕ_{fluo}	0.012	0.010	0.048	0.13
τ_{PL} /ns	n.d.	n.d.	27.9	9.7

n.d. not determined

3. Electrodeposition of gold nanoparticles on ITO substrates

Gold nanoparticles have been first electrodeposited on ITO by applying a constant reduction potential, varying from -0.7V to -0.9 V for a constant period of time. The corresponding chronoamperograms can be seen in figure S4. Then the coated ITO substrates were analyzed by SEM and the optical density measured as a control of the plasmon band position. The results are displayed in figure 4.

As already reported earlier by Lacroix[1], the density of nanoparticles on ITO increases with the negative overpotential, while the average size decreases at the same time (see table 3). This is because a more negative potential facilitates the nucleation but a larger density of nuclei is less favorable for the growth step. As a result, the plasmon band resonance is blue-shifted when the deposition potential is more negative.

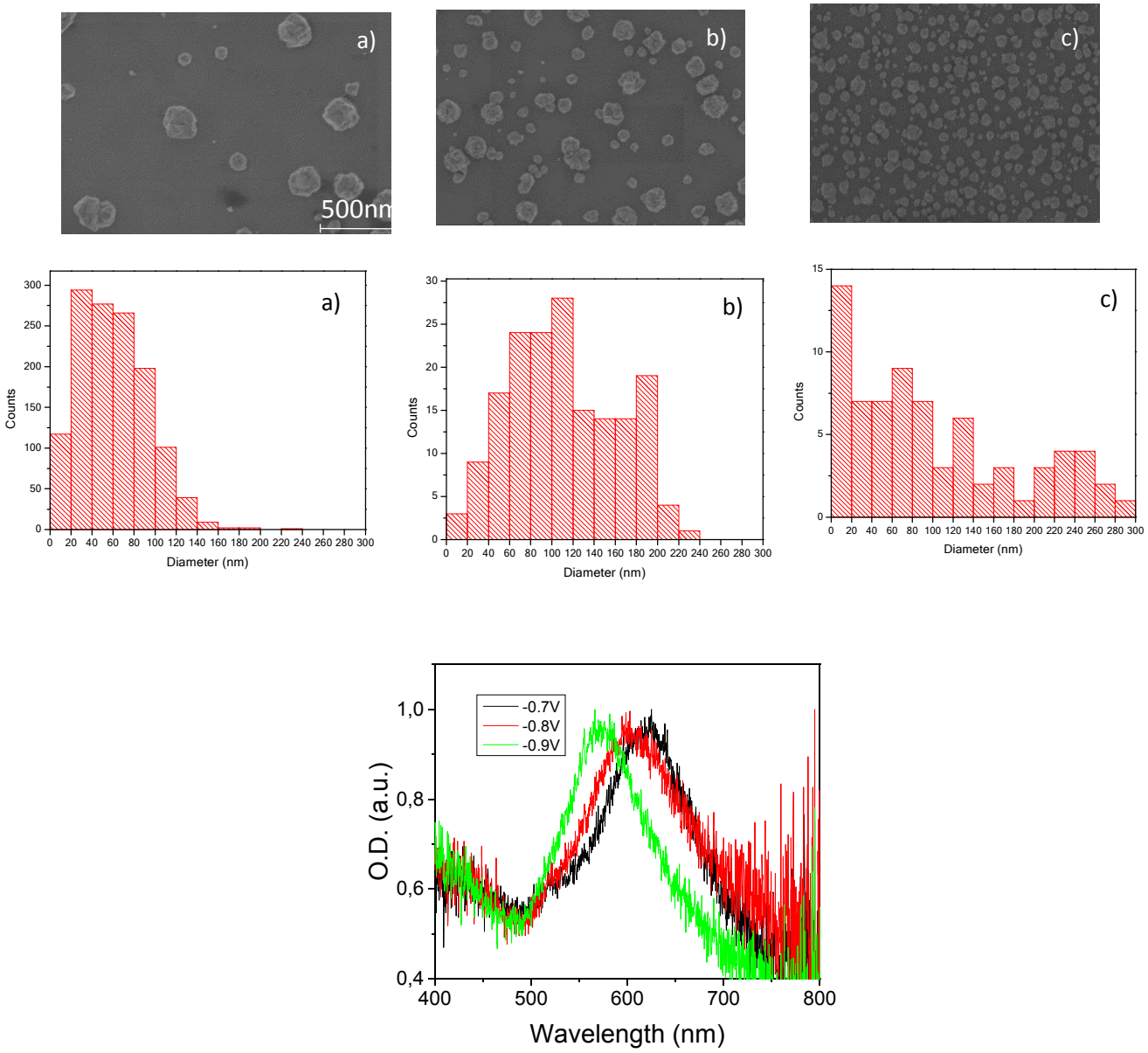

Figure 4: top: SEM images of electrodeposited AuNPs at a) -0.7 V, b) -0.8 V, c) -0.9 V w corresponding size histograms. Bottom: optical density of electrodeposited AuNPs at -0.7 V, -0.8 V, -0.9 V (all references vs Ag).

Table 3: Size characterization and surface plasmon resonance (LSPR) wavelengths as a function of applied potential.

Polarization potential /V	Number of particles	Average particle diameter /nm	Mean LSPR wavelength /nm	Average FWHM LSPR /nm
-0.7	24 ± 3	102.3 ± 81.1	631 ± 20	105 ± 7

-0.8	58 ± 8	111.9 ± 51.0	614 ± 11	104 ± 7
-0.9	259 ± 54	60.5 ± 31.9	580± 10	91 ± 5

The sample containing the highest amount of gold nanoparticles (-0.9 V) was selected for the ulterior tetrazine grafting, in order to maximize the amount of molecules present on the modified surface.

4. Grafting tetrazines on ITO-Au NP substrates

The grafting of **TzC$_6$SSTz** and **TzC$_6$Thioc** on ITO-Au NPs has been performed either by simple immersion or by applying a constant voltage leading to the reductive opening of the S-S bond. Then the resulting modified ITO-Au NP surfaces are analyzed by XPS, electrochemistry and fluorescence microscopy.

4.1 XPS

Elemental XPS analyses were preliminary performed to check the effectiveness of the grafting and assess the different grafting conditions of the tetrazine compounds on gold nanoparticles. Figure 5a shows a representative overall shape of the XPS curve, which did not show major changes regardless of the sample treatment, in the case of **TzC$_6$SSTz** grafting. Figure b shows the characteristic peaks of Au4f at 87.3eV and 83.5eV, which correspond to the $4f_{5/2}$ and $4f_{7/2}$ core level excitations respectively[6]. Even though the four nitrogen atoms of the tetrazine molecule are expected to be energetically equivalent, two components of the N1s core levels can be seen (Figure c). This effect was previously observed and attributed to interactions (such as hydrogen bonding) between the functionalized molecules grafted on the substrate[24]. The C1s spectrum (Figure d) shows the contribution of three different types of carbon: one at low energy (284.8 eV) and relatively in high proportion, which is attributed to the alkyl chain; the medium-sized peak at 286.5 eV corresponds to the carbons linked to oxygen, and the high-energy one at 288.2 eV corresponds to the most oxidized carbons of the *s*-tetrazine ring[24]. The core levels of S2p in figure 5e shows sulphur atoms in two different states: one at 161.8eV, which is generally attributed to chemically adsorbed S-Au bonds in self-assembled monolayers[25], and a second one at 163.5eV, assigned to physisorbed disulfide groups[26].

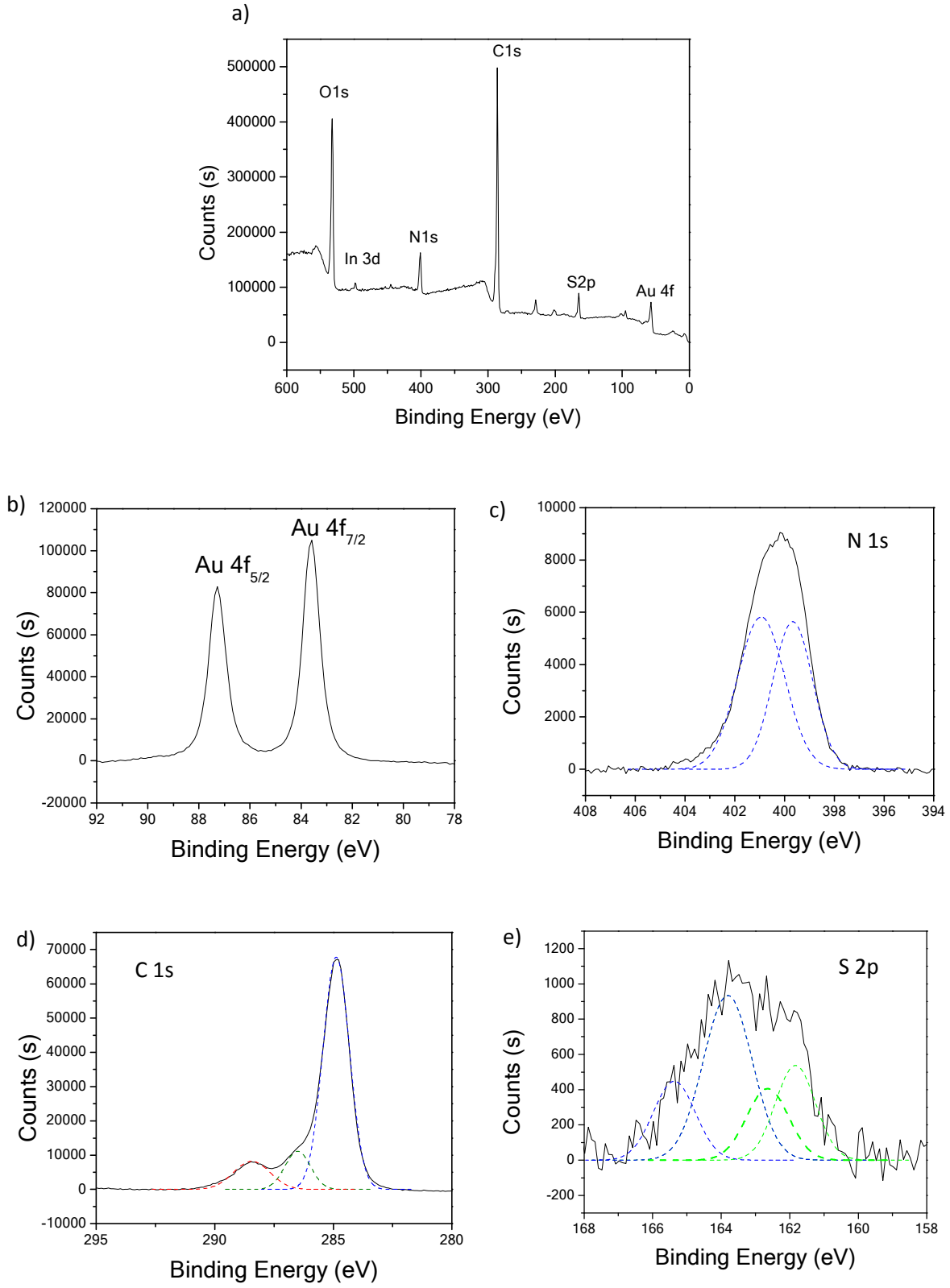

Figure 5: XPS analysis of the AuNP electrodes functionalized by **TzC_6SSTz**. a) Survey b) Au c) N d) C e) S. Black lines are spectra with background corrected, colored dashed lines are peak deconvolutions.

Table 4 shows the relative amounts of the various elements according to the functionalization treatment. It is evident that the electro-assisted methods promote a higher content of nitrogen and sulphur, whereas the gold content tends to decrease. This indicates that the molecule was properly grafted on the surface of the electrodes, with a higher amount for the electroassisted process.

Table 4: XPS analysis results for the main elements after ITO-Au NP functionalization by **TzC_6SSTz** with different methods. *The Au quantity was not identified properly.

Functionalization method	Element	Peak binding energy /eV	Relative atomic %
None	Au4f	83.60	5.22
	N1s	400.01	1.00
	C1s	284.82	35.10
	S2p	161.07	0.34
	S2p Ox	167.89	0.22
Immersion	Au4f	83.60	3.13
	N1s	400.13	3.79
	C1s	284.87	58.17
	Cl2p	198.71	0.56
	S2p	163.00	0.65
	S2p ox	168.85	0.50
-0.4V *vs* Ag	Au4f	84.11	2.66
	N1s	402.88	6.29
	C1s	285.52	66.00
	Cl2p	197.80	0.30
	S2p	163.42	1.11
	S2p ox	168.85	0.18
-0.6V *vs* Ag	Au4f	83.55	*
	N1s	400.22	8.26
	C1s	284.87	61.47
	Cl2p	198.21	0.86
	S2p	163.66	3.24

A similar XPS analysis was performed for the ITO-Au NP functionalized by **TzC$_6$TzThioc** at fixed potential. All the expected elements (Au, C, Cl, N and S) are actually detected. The relative proportions are given in table 5. The Cl/N ratio is slightly lower than the theoretical atomic composition but the presence of these two elements certify the proper grafting of the tetrazine compound on Au. The S2p signal shows two bands: one at high energy (S2p3B, 169 eV) corresponding to oxidized sulfur and another one at 163 eV due to reduced sulfur[27]. This latter band involves two types of sulfur atoms (S2p3 and S2p3A, see table 5) that can be assigned respectively to bound (S2p3A) and unbound (S2p3) atoms in reference to the grafting of thioctic acid on gold.[28] Compared to the disulfide sample, the atomic percentage of N and Cl is higher and the proportion of bound vs. unbound sulfur as well. These data are in favor of a better grafting when using the thioctic group as an anchoring function.

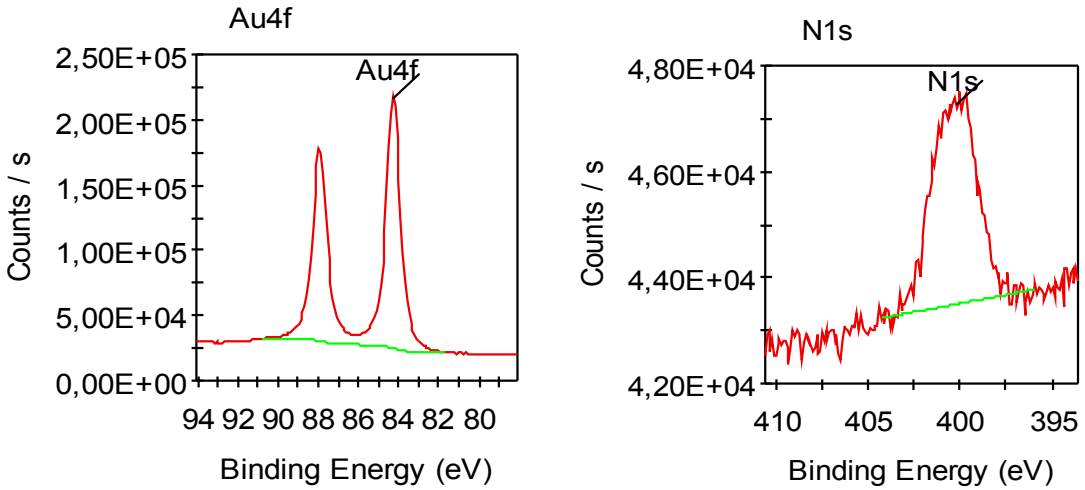

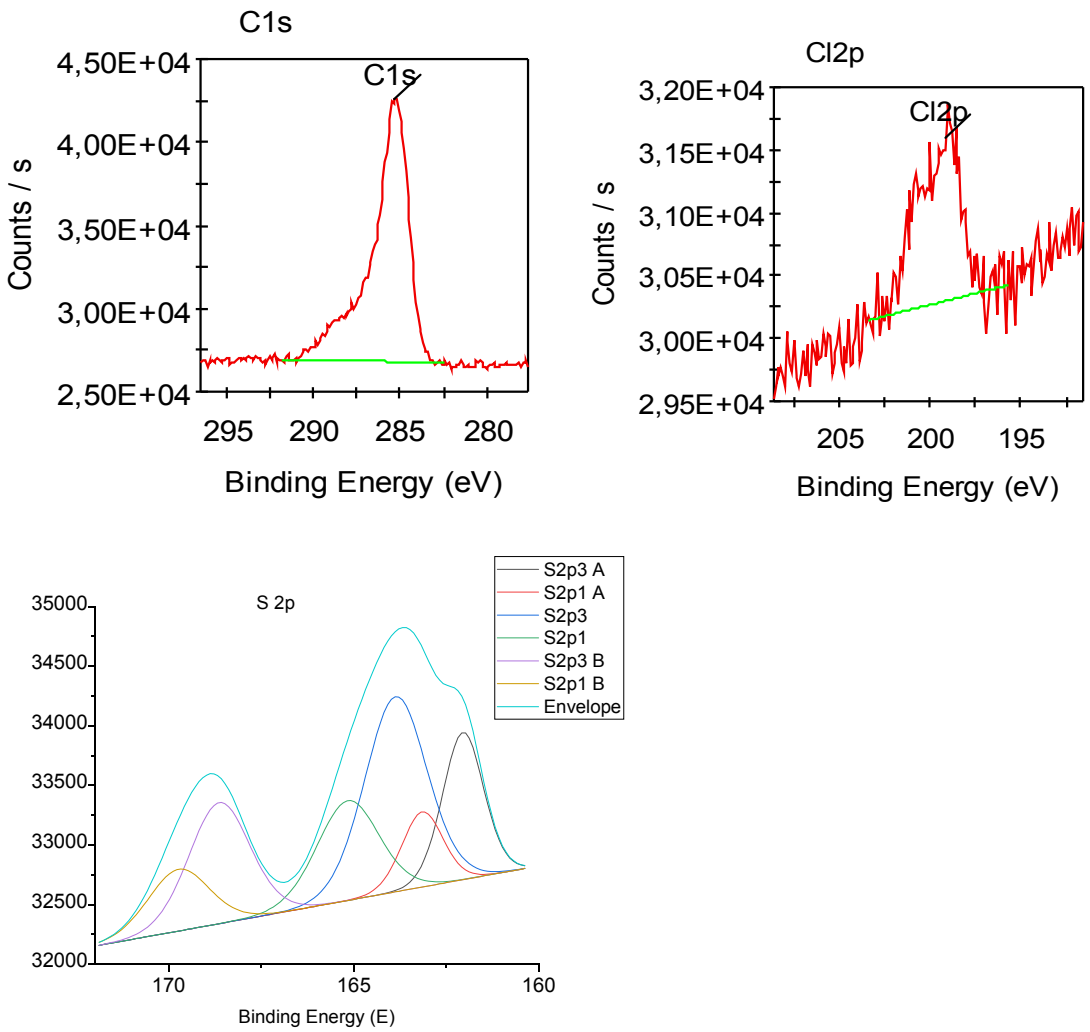

Figure 6: XPS analysis of ITO-Au NPs functionalized by **TzC$_6$Thioc**: C(1s), Cl(2p) and S(2p) signals.

Table 5: XPS composition of the **TzC$_6$Thioc** monolayer on ITO-Au NP.

Element	Peak Binding energy /eV	Atomic %
Au4f	84.26	9.60
C1s	285.28	26.28
Cl2p	199.15	0.89
N1s	400.21	4.93
O1s	530.57	54.65
S2p1	165.16	0.00
S2p1 A	163.15	0.00
S2p1 B	169.73	0.00

S2p3	163.86	1.73
S2p3 A	162.05	0.86
S2p3 B	168.63	1.06

4.2 Electrochemistry

Figure 7 shows the CVs of an ITO/AuNPs electrode functionalized by **TzC_6SSTz** via electro-assisted deposition (at -0.6 V *vs* Ag). The observed reduction peak is related to the reduction of the tetrazine to its radical anion form, which is reoxidized in the back scan. A more reversible redox signal can be seen in the case of **TzC_6Thioc** with 38 and 28 µC.cm^{-2} for the reduction and oxidation coulombic charges respectively. These values lead to a surface coverage of 3.9 10^{-10} mol cm^{-2} which is the expected order of magnitude for monolayers (2.4 molecules per nm^2). The proper immobilization of the molecule on the surface is verified by the linear relationship between peak current and scan rate (figure S6). The absence of diffusion limited regime indicates that the monolayer remains accessible to the electrolyte counter ions when the tetrazine unit is reduced.

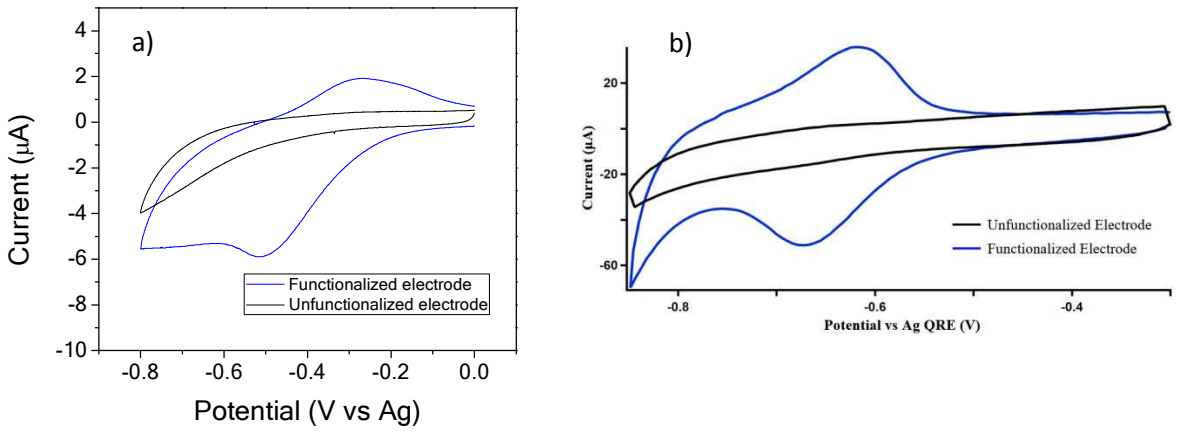

Figure 7: Cyclic voltammetry, comparison of bare (black trace) and a) **TzC_6SSTz** and b) **TzC_6Thioc** (blue traces) functionalized electrodes. Scan rate : 100 mV/s

The electron transfer kinetics associated with the reduction of the tetrazine units in the self-assembled monolayers on gold can be estimated by looking at the variation of peak potentials with the logarithm of scan rate as first demonstrated by Laviron.[29] Figure S7 shows the classical trumpet shape curve with the slope and crossing point of the linear asymptotes allowing to estimate the transfer coefficient α= 0.42 and the electron transfer rate constant k_s= 4 s^{-1}. This latter value is similar as the one obtained for ferrocene terminated alkylthiolates but with a much longer chain.[30] This corroborates the fact that

tetrazine redox units have intrinsic standard electron transfer rates which are significantly lower than those of very rapid redox systems like ferrocene. However, this value is sufficiently high to ensure that the SAM is well organized without too many defects.

4.3 Photophysics

The photoluminescence (PL) properties of the tetrazine derivatives grafted on Au NPs have been investigated using the set-up coupling fluorescence microscopy and electrochemistry (see SI for experimental details).

One of the main difficulties in characterizing the PL of grafted fluorophores on Au NPs ITO substrates is to cope with a very weak signal due to partial quenching of the emission by Au NPs, which makes the contribution of the PL substrate unneglectable. This was expected due to the overlap between the plasmon resonance band of the Au NPs and the emission spectrum of the fluorophore. Moreover, applying a continuous light flux results in the gradual bleaching of the fluorophores, possibly enhanced by their mutual vicinity on the surface in SAMs. Nevertheless, we can take benefit of this bleaching by comparing it to a non-functionalized substrate serving as a blank, in order to discriminate the contributions of the molecule and the substrate.

a) TzC_6SSTz

Figure 8 shows the steady state emission before and after bleaching of a reference sample of non-functionalized ITO/AuNPs with the one grafted with **TzC_6SSTz**. While the overall signal does not change with time in the reference, the functionalized one shows a decrease in intensity in the 530 to 630 nm range, which is precisely where we expect the tetrazine emission. The assignment of this intensity loss is confirmed when looking at the bleaching kinetics in the 530 to 650 nm range on one hand and from 700 to 900 nm on the other hand. Once again, the non-functionalized surface does not show any variation in fluorescence in both ranges, meaning that the signal actually comes from the substrate autofluorescence, whereas the electrodes functionalized with **TzC_6SSTz** show a decrease in fluorescence intensity only in the range of 530 to 650 nm (figure 7c-d). This illustrates how we can take benefit of the bleaching to extract the low fluorescence signal of the fluorescent monolayers on gold from the background.

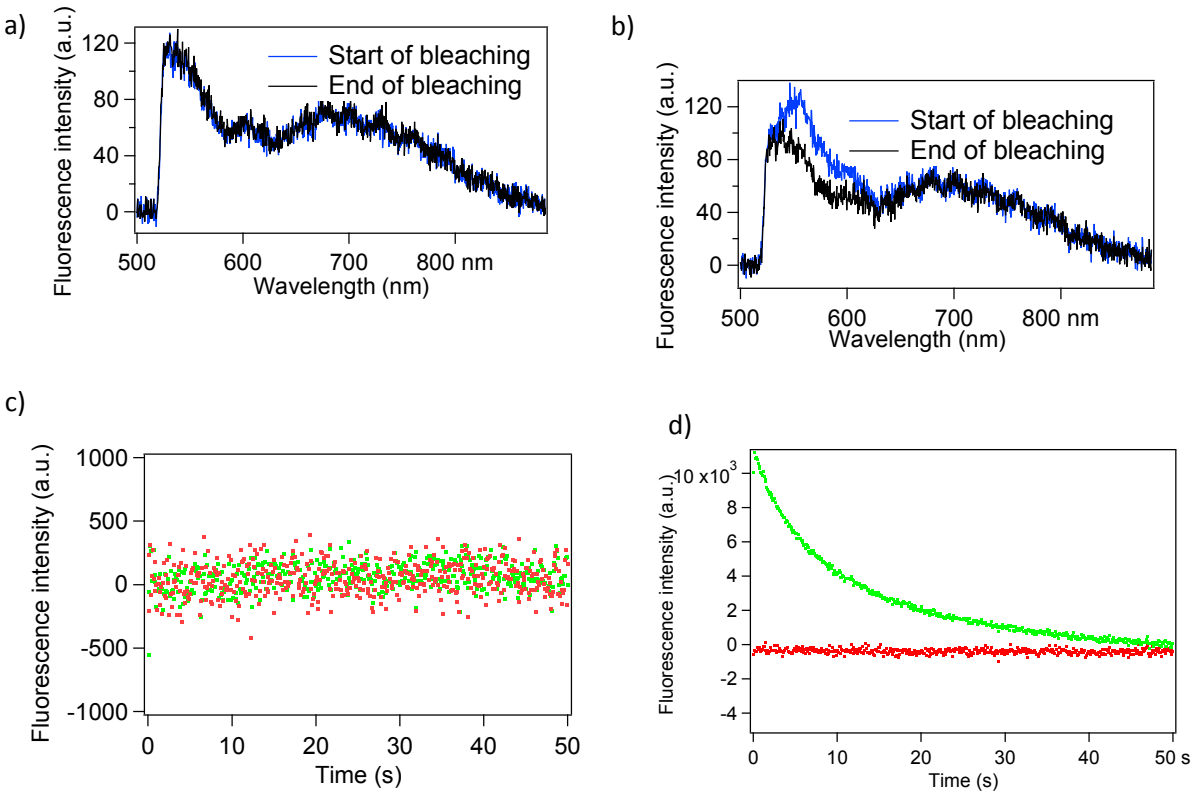

Figure 8: Steady state fluorescence emission after 5 minutes of bleaching of a) ITO/AuNPs reference sample and b) ITO/AuNPs-**TzC$_6$SSTz** functionalized samples. Fluorescence variation over time in different wavelength portions (530-650 nm in green, 700-900 nm in red) of c) ITO/AuNPs reference sample and d) ITO/AuNPs-**TzC$_6$SSTz** functionalized samples.

b) TzC$_6$Thioc

The same type of measurements has been performed on the ITO-AuNP modified by **TzC$_6$Thioc**. The emission band of the tetrazine fluorophore is this time clearly visible centered at 570 nm (figure 9a) because this compound has a higher quantum yield than the previous one. Continuous irradiation leads to a bleaching with a time evolution represented in figure 9b. Both the initial intensity and the bleaching rate are very different for the modified surface compared to the non-functionalized one serving as the reference. Figure S8 shows that the bleaching rate is strongly dependent on the excitation power: at low laser power, the fluorescence intensity remains constant over more than 100 s, while a gradual decrease of the emission intensity can be seen since the beginning at high laser power.

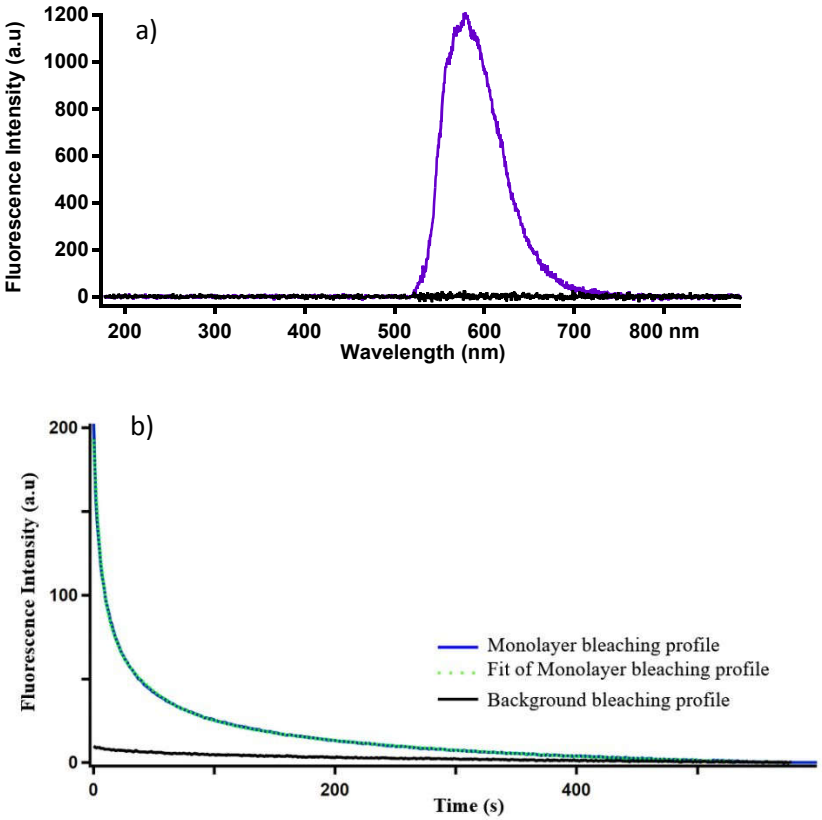

Figure 9: a) Emission spectra and b) bleaching kinetics of ITO-Au NP modified by **TzC$_6$Thioc**. The black trace shows the background contribution.

The decay profile of the emissive monolayer in figure 8b can be fitted by a multi-exponential function involving various characteristic times :

$$\sum_{i=1}^{n} A_i e^{\frac{-t}{\tau_i}}$$

In the present case, it has been noticed that the number of exponential functions necessary to fit the decay depends on the excitation power. At low fluence, a monoexponential decay is observed, while for higher fluence values three characteristic times are measured (see table 6).

Table 6: Characteristic times for bleaching decays according the excitation power.

Fluence /µW	τ_1 /s	τ_2 /s	τ_3 /s
20	-	-	210

200	3.7	41	248
2000	3.5	38	254

Finally, the influence of the deposition time has been investigated, by changing its value from 1h to 48h. The bleaching kinetics is very similar for all deposition times (see figure S9) and mainly dependent on the laser fluence as mentioned above. The comparison between the initial intensities show a slight increase up to an immersion time of 12h, which seems to correspond to the optimal coverage ratio. The trend is the same whatever the excitation power used (figure S10). We can this way estimate what is the immersion time necessary to get a full coverage of the gold nanoparticles by the fluorophores.

Conclusion

Various tetrazine derivatives incorporating disulfide and thioctic group for anchoring them on gold nanoparticles have been synthesized. These compounds are emissive and all tetrazine units are electroactive. The two compounds with the highest luminescence yields have been selected to be grafted on gold nanoparticles. In parallel, ITO electrodes have been decorated with gold nanoparticles either by simple immersion or by an electroassisted method. The functionalized ITO-gold nanoparticles surfaces were analyzed by XPS, electrochemistry and time-resolved fluorescence spectroscopy under microscope. Electrochemistry shows that redox active monolayers of the tetrazine have been deposited and a high electron transfer rate value. Fluorescence measurements demonstrate that these monolayers remain slightly emissive. The bleaching of the fluorophores in the monolayer deposited on gold has been analyzed according to the incident excitation power and immersion time. This latter does not seem to influence the bleaching kinetics. All these results show that tetrazine units remain emissive and electroactive once deposited on gold surface through thiol or thioctic anchoring groups.

Acknowledgments

Philippe DECORSE (ITODYS, Université Paris-Cité) is acknowledged for XPS measurements.

References

1. Nguyen, V.-Q.; Schaming, D.; Martin, P.; Lacroix, J.-C., Large-area plasmonic electrodes and active plasmonic devices generated by electrochemical processes. *Electrochimica Acta* **2015,** *179,* 282-287.

2. Dai, X. A.; Compton, R. G., Direct electrodeposition of gold nanoparticles onto indium tin oxide film coated glass: Application to the detection of arsenic(III). *Analytical Sciences* **2006,** *22* (4), 567-570.
3. Wang, L.; Mao, W.; Ni, D.; Di, J.; Wu, Y.; Tu, Y., Direct electrodeposition of gold nanoparticles onto indium/tin oxide film coated glass and its application for electrochemical biosensor. *Electrochemistry Communications* **2008,** *10* (4), 673-676.
4. Wang, J.; Wang, L.; Di, J.; Tu, Y., Electrodeposition of gold nanoparticles on indium/tin oxide electrode for fabrication of a disposable hydrogen peroxide biosensor. *Talanta* **2009,** *77* (4), 1454-1459.
5. Wang, Y.; Deng, J.; Di, J.; Tu, Y., Electrodeposition of large size gold nanoparticles on indium tin oxide glass and application as refractive index sensor. *Electrochemistry Communications* **2009,** *11* (5), 1034-1037.
6. Zhang, K.; Wei, J.; Zhu, H.; Ma, F.; Wang, S., Electrodeposition of gold nanoparticle arrays on ITO glass as electrode with high electrocatalytic activity. *Materials Research Bulletin* **2013,** *48* (3), 1338-1341.
7. Ngamaroonchote, A.; Muangnapoh, T.; Aroonyadet, N.; Kumnorkaew, P.; Laocharoensuk, R., Plasma-Etched Nanosphere Conductivity-Inverted Lithography (PENCIL): A Facile Fabrication of Size-Tunable Gold Disc Array on ITO-Coated Glass. *Advanced Materials Interfaces* **2018,** *5* (18).
8. Yang, J.; Strickler, J. R.; Gunasekaran, S., Indium tin oxide-coated glass modified with reduced graphene oxide sheets and gold nanoparticles as disposable working electrodes for dopamine sensing in meat samples. *Nanoscale* **2012,** *4* (15), 4594-4602.
9. Yang, J.; Ichii, T.; Murase, K.; Sugimura, H., Site-Selective Assembly and Reorganization of Gold Nanoparticles along Aminosilane-Covered Nano lines Prepared on Indium-Tin Oxide. *Langmuir* **2012,** *28* (20), 7579-7584.
10. Schaal, P. A.; Simon, U., Guided immobilisation of single gold nanoparticles by chemical electron beam lithography. *Beilstein Journal of Nanotechnology* **2013,** *4*, 336-344.
11. Bai, Z.; Tao, G.; Li, Y.; He, J.; Wang, K.; Wang, G.; Jiang, X.; Wang, J.; Blau, W.; Zhang, L., Fabrication and near-infrared optical responses of 2D periodical Au/ITO nanocomposite arrays. *Photonics Research* **2017,** *5* (4), 280-286.
12. Van-Quynh, N.; Dinh-Hai-Ngan, N.; Binh-Minh, N.; Thi-Mai-Thanh, D.; Lacroix, J.-C., Multiscale organization of a size gradient of gold nanoparticles in a honeycomb structure network. *Electrochemistry Communications* **2019,** *102*, 63-66.
13. Sabahat, S.; Janjua, N. K.; Brust, M.; Akhter, Z., Electrochemical fabrication of self assembled monolayer using ferrocene-functionalized gold nanoparticles on glassy carbon electrode. *Electrochimica Acta* **2011,** *56* (20), 7092-7096.
14. Dong, T.-Y.; Huang, C.; Chen, C.-P.; Lin, M.-C., Molecular self-assembled monolayers of ruthenium(II)-terpyridine dithiol complex on gold electrode and nanoparticles. *Journal of Organometallic Chemistry* **2007,** *692* (23), 5147-5155.
15. Capitao, D.; Limoges, B.; Fave, C.; Schollhorn, B., On the decisive role of the sulfur-based anchoring group in the electro-assisted formation of self-assembled monolayers on gold. *Electrochimica Acta* **2017,** *257*, 165-171.
16. Filippini, G.; Israeli, Y.; Goujon, F.; Limoges, B.; Bonal, C.; Malfreyt, P., Free Energy Calculations in Electroactive Self-Assembled Monolayers (SAMs): Impact of the Chain Length on the Redox Reaction. *Journal of Physical Chemistry B* **2011,** *115* (40), 11678-11687.
17. Blackman, M. L.; Royzen, M.; Fox, J. M., Tetrazine Ligation: Fast Bioconjugation Based on Inverse-Electron-Demand Diels−Alder Reactivity. *Journal of the American Chemical Society* **2008,** *130* (41), 13518-13519.
18. Audebert, P.; Miomandre, F., Electrofluorochromism: from molecular systems to set-up and display. *Chemical Science* **2013,** *4* (2), 575-584.
19. Aufaure, R.; Hardouin, J.; Millot, N.; Motte, L.; Lalatonne, Y.; Guenin, E., Tetrazine Click Chemistry for the Modification of 1-Hydroxy-1,1-methylenebisphosphonic Acids: Towards Bio-

orthogonal Functionalization of Gold Nanoparticles. *Chemistry-a European Journal* **2016,** *22* (45), 16022-16027.
20. Zhu, J.; Hiltz, J.; Lennox, R. B.; Schirrmacher, R., Chemical modification of single walled carbon nanotubes with tetrazine-tethered gold nanoparticles via a Diels-Alder reaction. *Chemical Communications* **2013,** *49* (87), 10275-10277.
21. Kirihara, M.; Asai, Y.; Ogawa, S.; Noguchi, T.; Hatano, A.; Hirai, Y., A Mild and Environmentally Benign Oxidation of Thiols to Disulfides. *Synthesis* **2007,** *2007* (21), 3286-3289.
22. MEADE, T. J. R., Matthew W.; HOLBROOK, Robert J. Gd(III)-DITHIOLANE GOLD NANOPARTICLE CONJUGATES. 2016.
23. Clavier, G.; Audebert, P., s-Tetrazines as Building Blocks for New Functional Molecules and Molecular Materials. *Chemical Reviews* **2010,** *110* (6), 3299-3314.
24. Li, Y.; Alain-Rizzo, V.; Galmiche, L.; Audebert, P.; Miomandre, F.; Louarn, G.; Bozlar, M.; Pope, M. A.; Dabbs, D. M.; Aksay, I. A., Functionalization of Graphene Oxide by Tetrazine Derivatives: A Versatile Approach toward Covalent Bridges between Graphene Sheets. *Chemistry of Materials* **2015,** *27* (12), 4298-4310.
25. Ivashenko, O.; van Herpt, J. T.; Feringa, B. L.; Browne, W. R.; Rudolf, P., Rapid reduction of self-assembled monolayers of a disulfide terminated para-nitrophenyl alkyl ester on roughened Au surfaces during XPS measurements. *Chemical Physics Letters* **2013,** *559*, 76-81.
26. Kumar, S.; Soni, S.; Danowski, W.; van Beek, C. L. F.; Feringa, B. L.; Rudolf, P.; Chiechi, R. C., Correlating the Influence of Disulfides in Monolayers across Photoelectron Spectroscopy Wettability and Tunneling Charge-Transport. *Journal of the American Chemical Society* **2020,** *142* (35), 15075-15083.
27. Dong, Y.; Abaci, S.; Shannon, C.; Bozack, M. J., Self-Assembly and Electrochemical Desorption of Thioctic Acid Monolayers on Gold Surfaces. *Langmuir* **2003,** *19* (21), 8922-8926.
28. Volkert, A. A.; Subramaniam, V.; Ivanov, M. R.; Goodman, A. M.; Haes, A. J., Salt-mediated self-assembly of thioctic acid on gold nanoparticles. *ACS nano* **2011,** *5* (6), 4570-80.
29. Laviron, E., General expression of the linear potential sweep voltammogram in the case of diffusionless electrochemical systems. *Journal of Electroanalytical Chemistry and Interfacial Electrochemistry* **1979,** *101* (1), 19-28.
30. Weber, K. S.; Creager, S. E., Reorganization energetics for ferrocene oxidation/reduction in self-assembled monolayers on gold. *Journal of Electroanalytical Chemistry* **1998,** *458* (1), 17-22.